

Demonstration of Time Delay Interferometry and Spacecraft Ranging in a Space-based Gravitational Wave Detector using the UF-LISA Interferometry Simulator

Shawn J. Mitryk* and Guido Mueller

*Department of Physics, University of Florida,
PO Box 118440, Gainesville, FL 32611-8440, USA*

(Dated: March 25, 2019)

Abstract

Space-based gravitational-wave observatories such as the Laser Interferometer Space Antenna (LISA) use time-shifted and time-scaled linear combinations of differential laser-phase beat signals to cancel the otherwise overwhelming laser frequency noise. Nanosecond timing precision is needed to accurately form these Time-Delay Interferometry (TDI) combinations which defines a ~ 1 meter requirement on the inter-spacecraft ranging capability. The University of Florida Hardware-in-the-loop LISA Interferometry Simulator (UFLIS) has been used to test Time-Delay Interferometry in a configuration which incorporates variable delays, realistic Doppler shifts, and simulated gravitational-wave signals. The TDI 2.0 combinations are exploited to determine the time-changing delays with nanosecond accuracy using a TDI-ranging reference tone. These variable delays are used in forming the TDI combinations to achieve the LISA interferometry sensitivity resulting from 10 orders of magnitude laser frequency noise cancellation.

PACS numbers: 04.80.Nn, 95.55.Ym, 07.87.+v, 07.60.Ly, 42.87.Bg, 07.05.Hd, 42.55.Xi, 42.60.Fc, 42.60.Mi

Keywords: LISA, LIGO, Gravitational Wave Detector, Time Delay Interferometry, TDI

INTRODUCTION

Future space-based gravitational wave (GW) interferometers [1, 2] will measure gravitational radiation from compact-star binaries and binary black hole mergers in the 0.1 mHz to 0.1 Hz frequency range, providing a new window through which to observe these astrophysical systems [3]. For the past ~ 20 years, the Laser Interferometer Space Antenna (LISA) has been the leading concept mission, studied and supported jointly by the European and US space agencies ESA and NASA [4, 5]. In 2011, the LISA-mission partnership was discontinued in favor of the development of post-LISA mission concepts and studies by both agencies independently, known as the New Gravitational Wave Observatory (NGO) in Europe [1] and the Space-based Gravitational Wave Observatory (SGO) in the US [2]. Most of these new concepts are variations of LISA using the same technologies under fairly similar conditions; in fact, most high-sensitivity post-LISA missions are similar to LISA while other versions use shorter arms, different orbits, and shorter lifetimes to save costs. In this paper, we utilize the LISA design, characteristics, and requirements as our baseline model although the results can easily be applied to future mission concepts.

LISA exploits a modified Michelson GW detection technique by taking one-way laser phase measurements between laser benches on three individual spacecraft (SC) (Fig. 1 [6]) to measure and extract the GW spacetime strain. The SC, defining the vertices of a triangular constellation, follow independent heliocentric orbits resulting in unequal, time-changing interferometer arm-lengths. Thus, the GW measurement sensitivity depends heavily on the ability to combine these individual SC data-sets to account for the laser frequency noise, clock noise, and spacecraft motion. These time-scaled and time-shifted linear combinations, referred to as time delay interferometry (TDI) combinations [7], complete the laser transfer chain, cancel the laser phase noise, and extract the GW strain information. LISA Simulator [8], Synthetic LISA [9], and LISA Tools [10] have produced numeric simulations of these data-sets for mock LISA data challenges (MLDCs) [11]. Hardware based laboratory experiments have also verified Sagnac-type TDI-combinations with clock noise corrections using a 1 meter test-bed. [12]

Taking the next step in validating the effectiveness of the TDI combinations, the University of Florida has constructed a hardware-based LISA simulator which utilizes a real-time digital electronic replication of the multi-second laser phase delays between individual laser

TABLE I. LISA Characteristics & Requirements

Characteristic	Specification
Laser Stab.	$\frac{280 \text{ Hz}}{\sqrt{\text{Hz}}} \sqrt{1 + \left(\frac{f_M}{f}\right)^4}$
PM Precision	$\frac{1 \mu\text{cycle}}{\sqrt{\text{Hz}}} \sqrt{1 + \left(\frac{f_M}{f}\right)^4}$
IMS Strain Sens.	$\frac{18 \text{ pm}}{\sqrt{\text{Hz}}} \sqrt{1 + \left(\frac{f_M}{f}\right)^4}$
DRS Accel. Noise	$\frac{3 fm/s^2}{\sqrt{\text{Hz}}} \sqrt{1 + \left(\frac{f}{f_H}\right)^4} \sqrt{1 + \left(\frac{f_L}{f}\right)^4}$
Ranging Accuracy	$\delta L = 1 \text{ meter}, \quad \delta \tau = 3.3 \text{ ns}$
Arm-Length	$L = 5.0 \pm 0.1 \text{ Gm}$
Light-Travel Delay	$\tau = 16.67 \pm 0.33 \text{ s}$
Relative Velocity	$v = \pm 20 \text{ m/s}, \quad \beta = \pm 66 \text{ ns/s}$
$f_L = 0.1 \text{ mHz}, f_M = 2.8 \text{ mHz}, f_H = 8 \text{ mHz}$	

benchtops while simultaneously taking low-frequency phasemeter (PM) measurements of LISA-like photodetector (PD) beatnotes [13]. Previous experiments have generated datasets and tested the capabilities of the TDI- X_1 combinations [14] which cancel the laser frequency noise in a static interferometer. Advancements to the simulator have provided the ability to model time-changing delays and incorporate the SC-motion induced laser phase coupling into the measurements. The following experiments use the TDI- X_2 combinations to cancel $\simeq 100 \text{ Hz}/\sqrt{\text{Hz}}$ laser phase noise in a LISA-like interferometer resulting in greater than 10 orders of magnitude noise suppression below 1 mHz and meeting the $18 \text{ pm}/\sqrt{\text{Hz}}$ LISA measurement sensitivity goal in a majority of LISA-like experiments. The analysis also shows how the time-varying inter-SC round-trip arm-lengths are ranged to an accuracy of < 2.0 meters utilizing a TDI-ranging [15] reference tone.

MODELING LISA

The sensitivity of the LISA detector is determined through a combination of requirements [6] which are defined to optimally observe scientifically interesting astrophysical sources while staying within the bounds of cost and feasibility. Each element in the LISA measurement chain has a pre-defined requirement (Table I) in order to meet the overall measurement sen-

sitivity. Based on these specifications, the dominant sensitivity-limiting terms in the LISA design are the disturbance reduction system's (DRS) acceleration noise at low frequencies, $f < 3$ mHz, and the interferometry measurement system's (IMS) displacement sensitivity at high frequencies, $f > 3$ mHz. The DRS is implemented to limit non-gravitational acceleration noise on the six, gravitationally sensitive, proof masses. This will be verified with a pre-LISA test mission, the LISA-Pathfinder [16]. The IMS is responsible for measuring the one-way differential length between these proof masses.

The LISA interferometry measurement scheme consists of six nearly-identical laser benchtops, two on each of the three SC. Each benchtop includes a pre-stabilized laser source, an optical bench, a proof-mass, a DRS, a fiber coupler to transfer the laser field between adjacent benchtops, and a telescope to transmit the laser field to the adjacent SC (Fig. 1) [6]. Each optical bench uses μ cycle PMs to measure the differential laser phase of heterodyned laser fields on three primary PDs. The measured signals are encoded with the local-SC to far-SC distance, s_{sr} , the local-SC to local-proof-mass distance, b_{sr} , and the differential laser phase induced by the fiber back-link between adjacent benchtops, f_{sr} . The TDI combinations of these observables are derived to complete the phase transfer chain and cancel the dominant laser phase noise.

To clarify the TDI analysis we consider two simplifications to the system. First, we assume that the counter-propagating fiber back-link terms, f_{sr} , can be measured and accounted for and, thus, we may treat the SC as having only one laser source [17]. Also, assuming the DRS system works well enough to shield the proof-masses from non-gravitational acceleration noise sources and that the local SC to local proof-mass distance can be accurately measured and accounted for, it is then justifiable to interpret the SC themselves as the interferometric GW proof masses and the b_{sr} terms can be neglected in the analysis as well [16]. This leaves the interesting TDI terms,

$$s_{sr}(t) = \phi_r(t) - \phi_s(\alpha_q(t - \tau_q(0))) + g_q(t), \quad (1)$$

$$s_{sr} = \phi_r - \phi_{s;q} + g_q, \quad (2)$$

or effectively, a comparative one-way measure of the local SC to far SC distance with a first-order velocity correction. In this notation ϕ_s is the phase of the 'sending' laser (from the adjacent SC), ϕ_r is the phase of the 'receiving' laser (on the local SC), and g_q is the GW modulated laser phase on the arm opposite SC_q . The light-travel time-delays between the

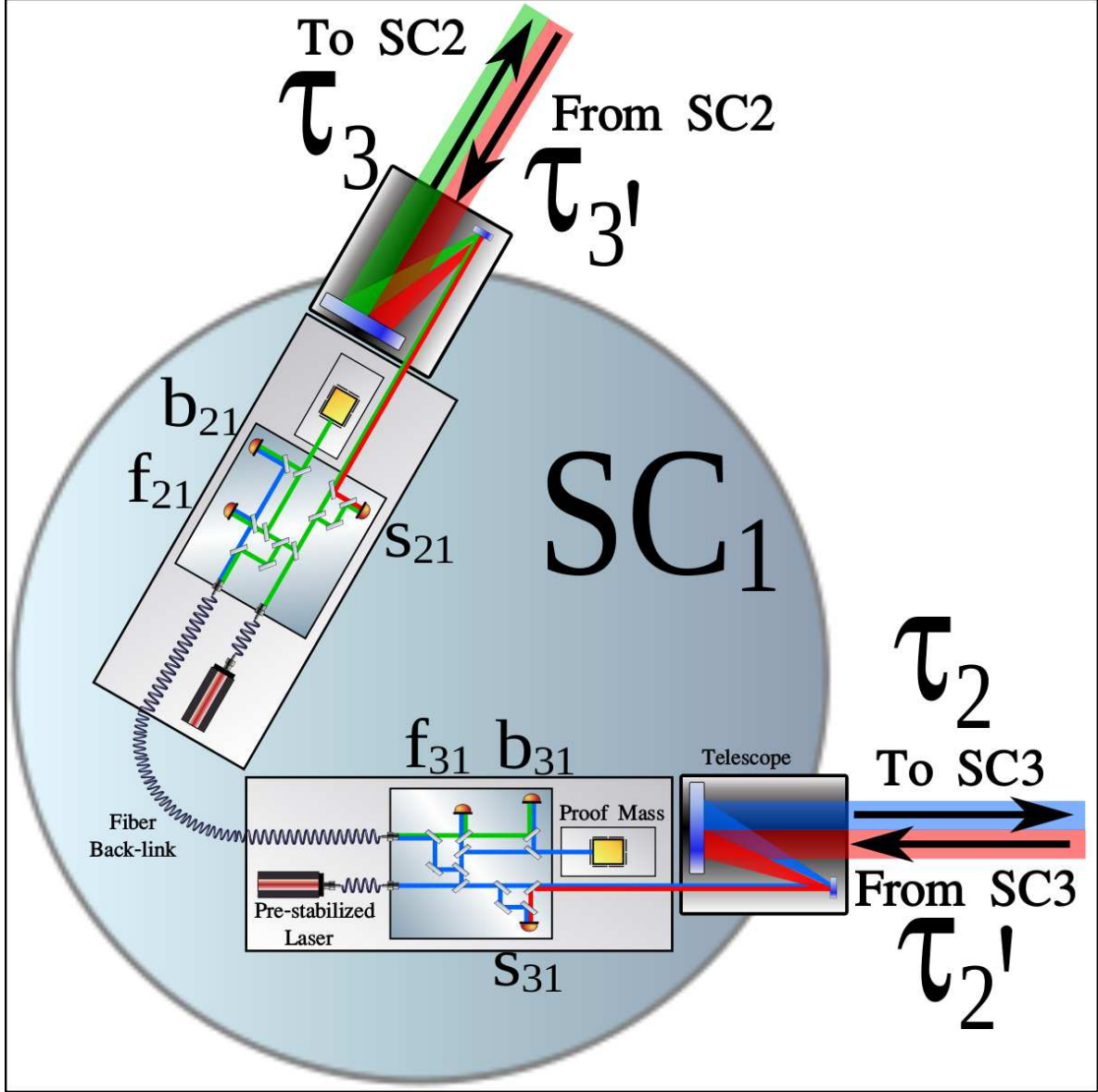


FIG. 1. Model of the LISA-IMS: The pre-stabilized lasers, proof-masses, optical benches, and inter-SC light field transfers of the LISA mission are illustrated. The spacecraft, SC_i , the associated light-travel time delays between the SC, $\tau_{q/q'}$, and the photodetector observables, s_{sr} , b_{sr} , and, f_{sr} , are labeled.

space-craft can written as $\tau_q(t) = \tau_q(0) + \beta_q t$ where $\tau_q(0)$ is the initial light-travel time-delay along the arm opposite SC_q , from SC_s to SC_r . $\beta_q = [1 - \alpha_q] = v_q/c$ where v_q is the differential position, or velocity, between SC_r and SC_s . The colon notation is used to transfer laser fields between moving frames by taking the time transformation, $t \rightarrow \alpha_q(t - \tau_q(0))$, as shown in Eq. 2, of which can be applied successively as in Eq. 4 [18]. Note that the counter-propagating

inter-SC light-travel time-delays along a single arm are not equal ($\tau_q(0) \neq \tau_{q'}(0)$) due to the orbital rotation of the constellation, although in this analysis, the first derivative is: $\beta_q = \beta_{q'}$ [19]. The prime notation refers to the different outgoing (un-primed) and returning (primed) light-travel-time laser phase delays. It is assumed that $|v_q| < 300 \text{ m/s}$, or, $|\beta| < 10^{-6}$; thus, 2^{nd} order special relativity corrections of order β^2 are negligible [18, 20].

TDI Theory

Choosing a master SC, SC_1 , as the interferometer vertex (beam-splitter), we can cancel the delayed $SC_{2/3}$ laser phase terms from the local, s_{s1} , signals and construct two differential, round-trip single-arm measurements by forming,

$$\Delta_s = s_{s1} + s_{1s;q'} \quad (3)$$

$$\Delta_s = \phi_1 - \phi_{s;q'} + (\phi_s - \phi_{1;q})_{;q'}$$

$$\Delta_s = \phi_1 - \phi_{s;q'} + \phi_{s;q'} - \phi_{1;qq'}$$

$$\Delta_s = \phi_1 - \phi_{1;qq'} \quad (4)$$

or, explicitly as a function of time:

$$\Delta_s(t) = s_{s1}(t) + s_{1s}(\alpha_{q'}(t - \tau_{q'}(0))) \quad (5)$$

$$\Delta_s(t) = \phi_1(t) + \phi_1(\alpha_q^2 t - \alpha_q^2 \tau_{q'}(0) - \alpha_q \tau_q(0))$$

where ϕ_1 is the master pre-stabilized laser phase.

In the special case where the total round trip delay-times are equal, $[\tau_2 + \tau_{2'}] = [\tau_3 + \tau_{3'}]$, and the differential SC velocities are zero, $\beta_2 = \beta_3 = 0$, the difference of the sensor signals,

$$X_0 = \Delta_2 - \Delta_3, \quad (6)$$

generates a standard equal-arm Michelson interferometer output, independent of laser phase noise. For LISA, this is rarely a reasonable laser phase cancellation technique since the arm-lengths are almost always un-equal. However, the TDI- X_1 combination [7], written as

$$X_1 = \Delta_2 - \Delta_3 - \Delta_{2;22'} + \Delta_{3;33'}, \quad (7)$$

replicates an equal-arm interferometer phase delay and cancels the common laser phase noise in the case where $[\tau_2 + \tau_{2'}] \neq [\tau_3 + \tau_{3'}]$ and $\beta_2 - \beta_3 \simeq 0$. Calculating the timing-error between

the $\phi_{1;33'22'}$ and $\phi_{1;22'33'}$ terms in Eq. 7, which result from laser phase transformation order of the $\Delta_{2;22'}$ and $\Delta_{3;33'}$ terms, we find:

$$\delta\tau = 4\tau|\beta_2 - \beta_3| \quad (8)$$

where τ is the mean one-way delay time ($\simeq 16.7$ s). Exploiting Eq. 11, derived in the next section, we can calculate the suppression limit of the TDI- X_1 combination, which fails to account for this SC-motion induced timing error, as [20]:

$$\tilde{X}_1 > 4\tau|\beta_2 - \beta_3|\dot{\phi}_1 \quad (9)$$

where $\dot{\phi}_1$ is the time-differentiated laser phase spectrum. Given a situation where this TDI- X_1 limit is large enough to restrain the IMS sensitivity, the TDI- X_2 combination,

$$\begin{aligned} X_2 = & \Delta_2 - \Delta_3 - \Delta_{2;22'} + \Delta_{3;33'} \\ & - \Delta_{2;33'22'} + \Delta_{3;22'33'} \\ & + \Delta_{2;22'22'33'} - \Delta_{3;33'33'22'} \end{aligned} \quad (10)$$

must be used to cancel the velocity coupled laser phase noise [18]. This TDI- X_2 combination accounts for the timing error of the TDI- X_1 combination by re-tracing and applying the TDI- X_1 laser phase-delay transfer chain through the constellation a second time.

Although the following analysis will focus on the TDI- X_2 velocity corrections, annual changes in β , or SC acceleration terms, may be accounted for with further expansion of these TDI combinations. Otherwise, and in order to utilize the TDI-ranging methods outlined below for LISA TDI data-analysis, the β value will have to be adjusted to avoid the acceleration-dependent accumulated error. Even though a continuous measure and correction to the β values is possible, these adjustments may also be accomplished by segmenting the data-analysis and adjusting the ranging functions used to evaluate the TDI combinations at regular intervals, in a worst case LISA-like scenario, every $\sqrt{\delta\tau T_{year}/(\beta \pi)} = \sqrt{3.3 \text{ ns} * 3.15 \times 10^7 \text{ s}/(66 \text{ ns/s} * \pi)} = 708 \text{ s}$ [9].

TDI Ranging

Until now, it has been assumed that we know the required interferometer arm-lengths and rate of change in order to form the TDI combinations but in practice this is not the

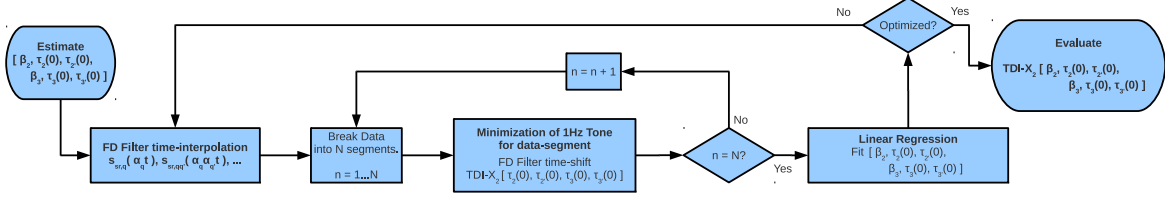


FIG. 2. Flow chart of the ranging-tone minimization process: This process minimizes the ranging tone and maximally constrains the six variable light travel time delays resulting in an optimized TDI- X_2 strain sensitivity. The results of this process for the different experimental configurations are in Table III and Table IV.

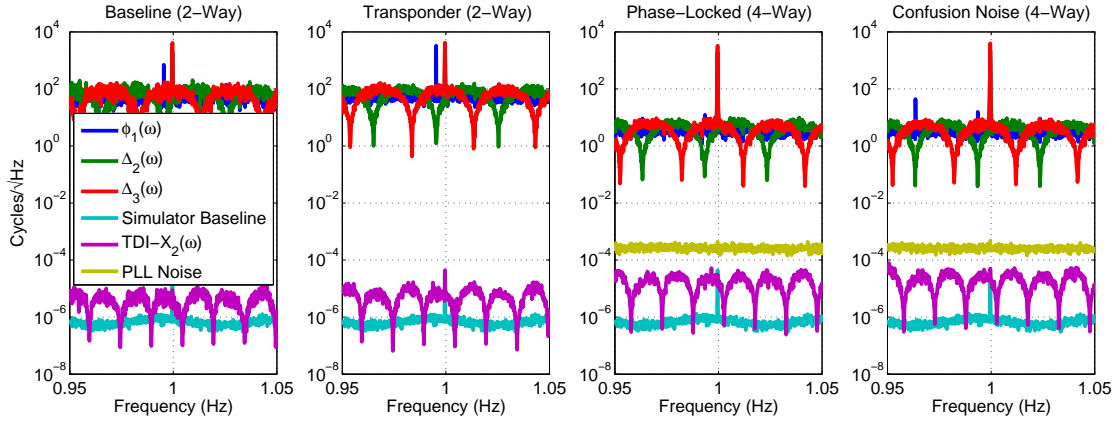


FIG. 3. Spectral magnitude tone suppression: The ranging tone modulated inputs are plotted along with the resulting TDI- X_2 combinations for the four different experiments outlined in Table II. The decreased round-trip timing accuracy of the Δ_2 arm as compared to the Δ_3 arm as shown in Table III and Table IV is likely due to the proximity of the nearest arm-zeros.

case. Two primary methods, pseudo-random noise (PRN) ranging [21] and TDI-ranging [15], have been proposed to measure these time-dependent arm-lengths. Extending the root mean squared (RMS) power minimization TDI-ranging methods outlined by Tinto in [15], this experiment will, instead, modulate the laser phase signals with ranging reference tones at frequencies outside of the LISA measurement band. The RMS power minimization around these relatively high-frequency tones avoids the displacement of the measured arm-lengths as a result of low-frequency GW signals [15] and provides an improved ranging precision beyond the inherent RMS laser noise cancellation resulting from the larger signal power at these chosen frequencies.

Using the Taylor approximation,

$$\begin{aligned} X_{Err} &\simeq \phi(t) - \phi(t + \delta\tau), \\ \tilde{X}_{Err} &\simeq [e^{-i\omega t} - e^{-i\omega(t+\delta\tau)}]\tilde{\phi}, \\ |\tilde{X}_{Err}| &\simeq \omega\delta\tau|\tilde{\phi}|, \end{aligned} \tag{11}$$

for $\omega\delta\tau \ll 1$, we can estimate a simplified but reasonable measure of the arm-lengths through the cancellation of these ranging tones using the TDI combinations to an accuracy of:

$$\delta L = \delta\tau c \simeq \frac{c}{2\pi f_{Tone}} G_{Tone}, \tag{12}$$

where f_{Tone} is the ranging-tone modulation frequency (1 Hz for these experiments) and G_{Tone} is the tone suppression magnitude when evaluated with the TDI combination. Generally, the cancellation of the local laser signal's ranging tones, $\phi_1(t)$, from the far s_{sr} signals in the TDI-X combinations (Eq. 7, 10) constrains the one-way outgoing delay times, $\tau_2(t)$ and $\tau_3(t)$, while the cancellation of the far laser signal's tones, $\phi_2(t)$ and $\phi_3(t)$, from the local s_{sr} signals constrains the incoming delay times, $\tau_{3'}(t)$ and $\tau_{2'}(t)$, respectively. Exploiting the phase-locking methods outlined in [22] such that $s_{12} \simeq s_{13} \simeq 0$ or, equivalently, $\phi_2 = \phi_{1;3'}$ and $\phi_3 = \phi_{1;2'}$, we can transfer the local laser phase data and phase stability to the far lasers and constrain the round trip delay times:

$$\tau_{22'}(t) = \alpha_2^2 t - \alpha_2^2 \tau_{2'}(0) - \alpha_2 \tau_2(0), \tag{13}$$

$$\tau_{33'}(t) = \alpha_3^2 t - \alpha_3^2 \tau_{3'}(0) - \alpha_3 \tau_3(0), \tag{14}$$

using a local, $\phi_1(t)$, ranging tone only.

Although some prior estimate of the arm-lengths will likely exist, the analysis in this paper will assume no previous knowledge of the 6-variable time-dependent round-trip arm-lengths, $\tau_{22'}(t)$ and $\tau_{33'}(t)$, and will determine these arm length functions using a 1 Hz laser frequency modulation with an amplitude of 500 Hz. Note that the ranging tone should not be placed at a frequency which is near an integer multiple of the interferometer arms' inverse round-trip delay time to avoid the inherent tone cancellation along a single arm as shown in Fig. 3. This local ranging tone will provide constraints on the round trip delay times only. Since the far laser phase signals in this experiment are not modulated with ranging tones but rather, phase locked [22], the one-way delay times are constrained using the TDI-ranging

methods outlined by Tinto [15] through the minimization of the PLL’s residual phase RMS power in the TDI- X_2 combination.

As shown in Fig. 2, initially assuming the arm-lengths are constant ($\beta = 0$) a four-dimensional sweep of the ‘time-space’ defined by $\tau_2(0)$, $\tau_{2'}(0)$, $\tau_3(0)$, and $\tau_{3'}(0)$ is performed using a 51-point Lagrange fractional delay (FD) filter [23] which determines the values which minimize RMS power near the 1 Hz frequency-modulated ranging tone in the TDI- X_2 combination. Generally, depending on the pre-stabilized laser noise and phase locking configuration, the delay times must be measured with a 10^{-8} resolution [6, 22]. Therefore, to make data analysis more efficient, rather than evaluating the 10^8 possible values along each of the 4 delay-dimensions, the time-delay determination is performed using an algorithmic scan with successively finer time-delay mesh grids until the ranging tone is minimized and dominated by the noise floor of the IMS measurement.

Using this scanning process, we determine an initial measure of the round-trip delay offsets, $\tau_{22'}(0)$ and $\tau_{33'}(0)$, which minimize the ranging tone for small data-segments along a continuous data-set. The fitted slope of these offsets evaluates a first-order approximation of β and the time-dependent arm-lengths. Applying the β -value dependent time-expansion or time-contraction to the s_{sr} signals using time-varying FD interpolation [23], the process is repeated iteratively, further optimizing the arm-length functions as shown in Fig. 2. Finally, the delay functions using the fitted, $\beta_2, \beta_3, \tau_2(0), \tau_{2'}(0), \tau_3(0)$, and $\tau_{3'}(0)$, values, are used to evaluate the TDI- X_2 combination along the entire data-set. The results produce a measure of the round-trip arm-lengths and place constraints on the one-way arm-lengths to an accuracy beyond the ranging requirements, thus, removing the sensitivity-limiting laser and PLL phase noises sources and idealizing the total interferometer strain precision.

LISA SIMULATOR BENCHTOP

The University of Florida LISA Simulator (UFLIS) benchtop (Fig. 4) consists of four lasers, three of which, Laser-1 (L_1), Laser-2 (L_2), and Laser-3 (L_3) represent the lasers on each of the SC in the LISA constellation. Laser beatnotes are formed between each of these laser fields and a global reference laser (L_R), acting as an optical clock against which each individual laser phase is measured. Combinations of these PD measurements cancel the common L_R phase noise. L_R and L_1 are stabilized through Pound-Drever-Hall (PDH)

TABLE II. TDI Experimental Characteristics: Four 40000 s experiments are performed with increasingly more complicated, yet more LISA-like, characteristics. The static transponder experiment provides us with a baseline measure of the experimental setup’s noise performance. The dynamic transponder experiment demonstrates the ability to determine and account for the time-changing delay-times. The phase-locked LISA-like experiment proves the ability to remove independent SC noise sources and constrain one-way delay times. Finally, the confusion noise experiment verifies that the TDI-ranging capability will not be limited by low-frequency LISA noise sources.

Simulation Name	s_{1r}	β (ns/s)	Verification Signal
Static Transponder	$s_{1r} \simeq 0$	$\beta_2 = \beta_3 = 0$	6.22 mHz Binary
Dynamic Transponder	$s_{1r} \simeq 0$	$\beta_2 = -100, \beta_3 = +150$	6.22 mHz Binary
Dynamic LISA-like	$s_{1r} \simeq \phi_{PLLr}$ $\simeq (1.0/f) \text{ mcycle}/\sqrt{\text{Hz}}$	$\beta_2 = -100, \beta_3 = +150$	6.22 mHz Binary
Dynamic LISA-like with Confusion-Noise	$s_{1r} \simeq \phi_{PLLr}$ $\simeq (1.0/f) \text{ mcycle}/\sqrt{\text{Hz}}$	$\beta_2 = -100, \beta_3 = +150$	6.22 mHz Binary + Confusion-Noise

stabilization [24] using ultra-low expansion reference cavities to achieve a $\simeq 100 \text{ Hz}/\sqrt{\text{Hz}}$ pre-stabilized laser noise as shown in Fig. 6. Even though a lower laser frequency noise is achievable [13], it is intentionally spoiled to display the suppression capabilities of the TDI combinations.

Phasemeter

The phasemeter is used to measure the phase of a 2-20 MHz PD beatnote signal to an accuracy of $\simeq 1 \mu\text{cycle}/\sqrt{\text{Hz}}$ (Table I). The beatnote is sampled using a 14-bit analog-to-digital Converter (ADC) at a rate of 40 MHz. The sampled signal is processed by a field programmable gate array (FPGA) programmed with a digital phase-lock loop (PLL). The digital PLL’s feedback signal is down-sampled to a rate of 19.1 Hz and relayed to a data-processing computer. Using entangled phase and differential PM measurements it has been determined that the PM is limited by $\tilde{\phi}_{ADC}$ (Fig. 8), a combination of frequency-dependent ADC timing jitter ($\delta t = 35/\sqrt{f} \text{ fs}/\sqrt{\text{Hz}}$), RF-transformer phase dispersion, and amplitude

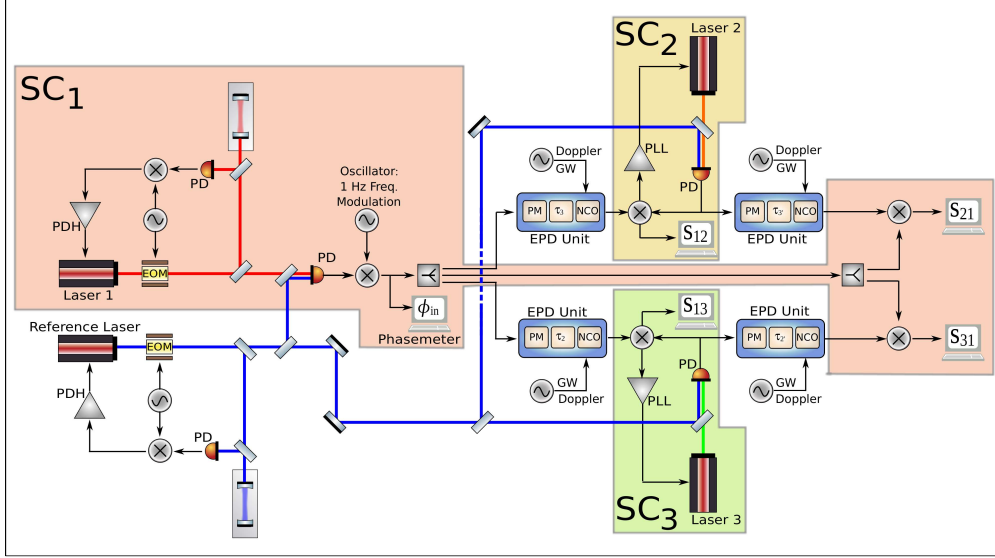


FIG. 4. Experimental Model of the LISA Interferometry Benchtop: The arrangement of the laser phase sources, EPD units, phase-lock loops, PD signal beatnotes, and PM measurements which are used to emulate the LISA-IMS in our experiments are presented. The measured s_{sr} signals are used to form the TDI combinations.

noise [25]. One may write the PM measurement output as

$$\phi_{PM}(t) = \phi_{in}(t) + \frac{f_{in}}{f_{clk}} \phi_{clk}(t) + \phi_{ADC}(t), \quad (15)$$

where ϕ_{in} is the phase information on the f_{in} -frequency beat-note, ϕ_{clk} is the phase noise of the f_{clk} -frequency sampling clock, and ϕ_{ADC} are the ADC-noise sources mentioned above. Note the coupling of the clock's phase noise into the measurement. PM measurements taken on different LISA SC will be clocked using different ultra-stable clock sources requiring the need for clock-noise transfers between SC to remove these terms [26]. Although the following TDI experiments described below use a single clock source, the TDI combinations will still require clock-noise corrections to account for the time-shifted PM clock noise terms. This is discussed in the following section.

Electronic Phase Delay Unit

The EPD unit simulates the characteristics of the laser phase transmission between the SC, including the time-varying light travel time, laser frequency Doppler shift, and laser phase gravitational wave modulations, using a high-speed digital signal-processing (DSP)

system. The front end is a fast PM, similar to the PM described above, with a data rate of 19.53 kHz instead of 19.1 Hz. The PM data is interpolated to time-lead or time-lag the phase information, producing a linear variation in the time-delay. GW signals and a Doppler offset are added to the interpolated phase information before it is used to drive a numerically controlled oscillator (NCO). Completing the laser phase transmission replication, the NCO output is regenerated using a 16-bit digital-to-analog converter (DAC) using the same clock-source as the PM. After accounting for the clock noise coupling and Doppler shifts, we can write the EPD unit's output as,

$$\begin{aligned}
\phi_{EPD}(t) = & \phi_{in}(t - \tau(t)) \\
& + \phi_{ADC}(t - \tau(t)) + \phi_{DAC}(t) \\
& + \phi_{Clk:ADC}(t - \tau(t)) - \phi_{Clk:DAC}(t) \\
& + \frac{f_{in} \pm f_{Dop}}{f_{Clk}} [\phi_{Clk}(t - \tau(t)) - \phi_{Clk}(t)].
\end{aligned} \tag{16}$$

$\phi_{in}(t)$ is the phase evolution of the beatnote with a frequency of $f_{in} = 2 - 20$ MHz. The beat signals are measured and regenerated with respect to a single clock, $\phi_{Clk}(t)$, at the DSP system clock frequency of $f_{Clk} = 40$ MHz. The phase noise of this clock enters as phase variations between the sampling and the f_{Dop} Doppler shifted regeneration of the input signal during the time-varying time-delay, $\tau(t) = \tau(0) + \beta t$. The single clock source is split and distributed between the sampling ADC and regeneration DAC causing an additional phase error, $\phi_{Clk:ADC}(t - \tau(t)) - \phi_{Clk:DAC}(t)$. The sampling (ϕ_{ADC}) and regeneration (ϕ_{DAC}) processes add additional converter-noise contributions. It has been determined using two different sampling and regeneration clock sources that the limiting noise source on the EPD unit (Fig.8) is the differential clock phase noise, $\phi_{Clk:ADC,\tau(t)} - \phi_{Clk:DAC}$, caused by errors in the clock distribution [25]. Note, as one may check, that the clock noise terms themselves, $\phi_{Clk}(t)$ in Eq. 16, will cancel when measured with phasemeters (Eq. 15) and evaluated in the TDI combinations (Eq. 7, 10).

Experimental Setup

The laser benchtop, PMs, and EPD units are combined to recreate the LISA-IMS (Fig. 4). The L_1/L_R differential beatnote phase represents the pre-stabilized ‘input’ noise. This PD signal is electronically mixed with a 1 Hz frequency-modulated oscillator to add a ranging-

tone and produce the input laser phase signals. Replicating an interferometer beam-splitter, these signals are electronically split and processed by the EPD units to simulate the outgoing-field inter-SC light transmission. The EPD-processed signal is mixed with each of the $L_{2/3}/L_R$ beatnotes ‘on the far spacecraft’ to produce the s_{12} and s_{13} PM signals. These delayed signals are also used to phase-lock $L_{2/3}$, transferring the L_1 stability to these lasers [22]. The $L_{2/3}/L_R$ beatnotes are again processed by EPD units, simulating the returned-field inter-SC light transmission. Finally, the local differential L_1/L_R input phase signal is mixed with the delayed $L_{2/3}/L_R$ beatnotes to produce the s_{21} and s_{31} PM signals.

Implementing this experimental model, four measurements are performed as outlined in Table II. In the transponder measurements, rather than phase-locking the outgoing-field’s EPD signal, it is transferred directly to the return-field’s EPD unit as though it were reflected off of a moving mirror; accordingly, these TDI experiments may completely neglect the s_{1r} terms while ranging is only required for the round-trip delay times, $\tau_{22'}(t)$ (Eq. 13) and $\tau_{33'}(t)$ (Eq. 14), instead of all four one-way delay times. For all measurements presented, the arm-lengths are chosen as $\tau_2 \simeq \tau_{2'} \simeq 16.55$ s and $\tau_3 \simeq \tau_{3'} \simeq 16.75$ s to maximize the unequal arm-length mismatch. The relative spacecraft velocities for the different measurements are shown in Table II. They are artificially large to increase the $|\beta_2 - \beta_3|$ limitations (Eq. 9) for the TDI- X_1 combination and to prove the ability of the TDI- X_2 to remove the differential velocity dependent noise from the TDI- X_1 combination. Doppler shifts of -2.0 MHz and +3.0 MHz are applied in order to produce the necessary MHz beatnote observables. A frequency modulated 6.22 mHz verification binary GW signal with an amplitude of $\delta f_{GW} = 2 \mu\text{Hz}$ is injected into all four measurements to verify GW extraction. This frequency modulation equates to a phase modulation amplitude of $\delta\phi_{GW} = \delta f_{GW}/(2\pi f) = 51.2 \mu\text{cycles}$ resulting in a one-way strain amplitude of $\delta h_{Arm} = \lambda\delta\phi_{GW}/[c\tau] = 1.1 \times 10^{-20}$. The resulting GW strain amplitude $\delta h_{LISA} = 2\delta h_{Arm}/\sin(60^\circ) = 2.5 \times 10^{-20}$ is a factor of 100 larger than expected for the RX J0806.3+1527 AM CVn binary [27]. The factor of 2 in this relationship accounts for the two interferometer arms while the factor of $\sin(60^\circ)^{-1}$ accounts for the non-orthogonality of the LISA interferometer arms. Finally, a mock-confusion noise is added to the signals to demonstrate that this low-frequency noise will not limit the ranging capabilities.

The following experimental results are averaged over six, 10000 s, data-segments during the course of a continuous 40000 s experimental run-time.

TABLE III. Transponder Ranging Precision

TDI Experiment Name			
TDI-Ranging Constraint			
Iteration (TDI combination)	β	$\tau_{22'}(0), \tau_{33'}(0)$	$\delta\tau_{22'}, \delta\tau_{33'}$
Static Transponder			
Round-trip Ranging			
1 (TDI 1.0)	$2\beta_2 = -44.5 \text{ fs/s} \pm 20.9 \text{ fs/s}$	$\tau_{22'}(0) = 33.55204887148 \text{ s} \pm 0.23 \text{ ns}$	$\delta\tau_{22'} = 0.54 \text{ ns}$
	$2\beta_3 = -46.3 \text{ fs/s} \pm 12.5 \text{ fs/s}$	$\tau_{33'}(0) = 33.15222859583 \text{ s} \pm 0.14 \text{ ns}$	$\delta\tau_{33'} = 0.32 \text{ ns}$
1 (TDI 2.0)	$2\beta_2 = -41.0 \text{ fs/s} \pm 21.2 \text{ fs/s}$	$\tau_{22'}(0) = 33.55204887151 \text{ s} \pm 0.24 \text{ ns}$	$\delta\tau_{22'} = 0.55 \text{ ns}$
	$2\beta_3 = -46.3 \text{ fs/s} \pm 12.7 \text{ fs/s}$	$\tau_{33'}(0) = 33.15222859579 \text{ s} \pm 0.14 \text{ ns}$	$\delta\tau_{33'} = 0.33 \text{ ns}$
Dynamic Transponder			
Round-trip Ranging			
1 (TDI 2.0)	$2\beta_2 = -200.247 \text{ ns/s} \pm 100 \text{ ps/s}$	$\tau_{22'}(0) = 33.5518847 \text{ s} \pm 2.3 \mu\text{s}$	$\delta\tau_{22'} = 7.5 \mu\text{s}$
	$2\beta_3 = +300.056 \text{ ns/s} \pm 95 \text{ ps/s}$	$\tau_{33'}(0) = 33.1525027 \text{ s} \pm 2.2 \mu\text{s}$	$\delta\tau_{33'} = 7.0 \mu\text{s}$
2 (TDI 2.0)	$2\beta_2 = -199.9998668 \text{ ns/s} \pm 80 \text{ fs/s}$	$\tau_{22'}(0) = 33.5519484187 \text{ s} \pm 1.8 \text{ ns}$	$\delta\tau_{22'} = 5.9 \text{ ns}$
	$2\beta_3 = +300.0001130 \text{ ns/s} \pm 23 \text{ fs/s}$	$\tau_{33'}(0) = 33.1523897572 \text{ s} \pm 0.51 \text{ ns}$	$\delta\tau_{33'} = 1.7 \text{ ns}$
3 (TDI 2.0)	$2\beta_2 = -200.0000058 \text{ ns/s} \pm 8.9 \text{ fs/s}$	$\tau_{22'}(0) = 33.55194832884 \text{ s} \pm 0.20 \text{ ns}$	$\delta\tau_{22'} = 0.65 \text{ ns}$
	$2\beta_3 = +300.0001361 \text{ ns/s} \pm 4.5 \text{ fs/s}$	$\tau_{33'}(0) = 33.15238977691 \text{ s} \pm 0.10 \text{ ns}$	$\delta\tau_{33'} = 0.33 \text{ ns}$

TDI RESULTS

Static Arm Transponder (Baseline)

We first re-establish [14] a baseline ranging and measurement precision with static arm-lengths ($\beta = 0$), utilizing the PD measurements of s_{21} and s_{31} and assuming $s_{12}, s_{13} \simeq 0$ when evaluating the TDI combinations. The 40000 s data-set is broken into 40, 1000 s segments. The first iteration and linear regression of the ranging process described in Fig. 2 produces a slope error (constraint on the arm-length velocities), of $|2\beta| < 50 \text{ fs/s}$ and a variance (round-trip ranging accuracy) of 0.6 ns ($\sim 0.18 \text{ m}$) as shown in Table III. In this experiment, we note that the TDI- X_1 combination's ranging-tone minimization produces the same result as the TDI- X_2 combination to within the measurement error. If $\beta \neq 0$, this would not be the case since the ranging tone minimization using the TDI- X_1 combination would be limited by Eq. 9 and would tend to calculate the mean delay for a particular data-segment.

Using the calculated values we form the TDI- X_1 and TDI- X_2 combinations for the entire data-set. The raw TDI results, as plotted in Fig. 5, show the laser noise cancellation and

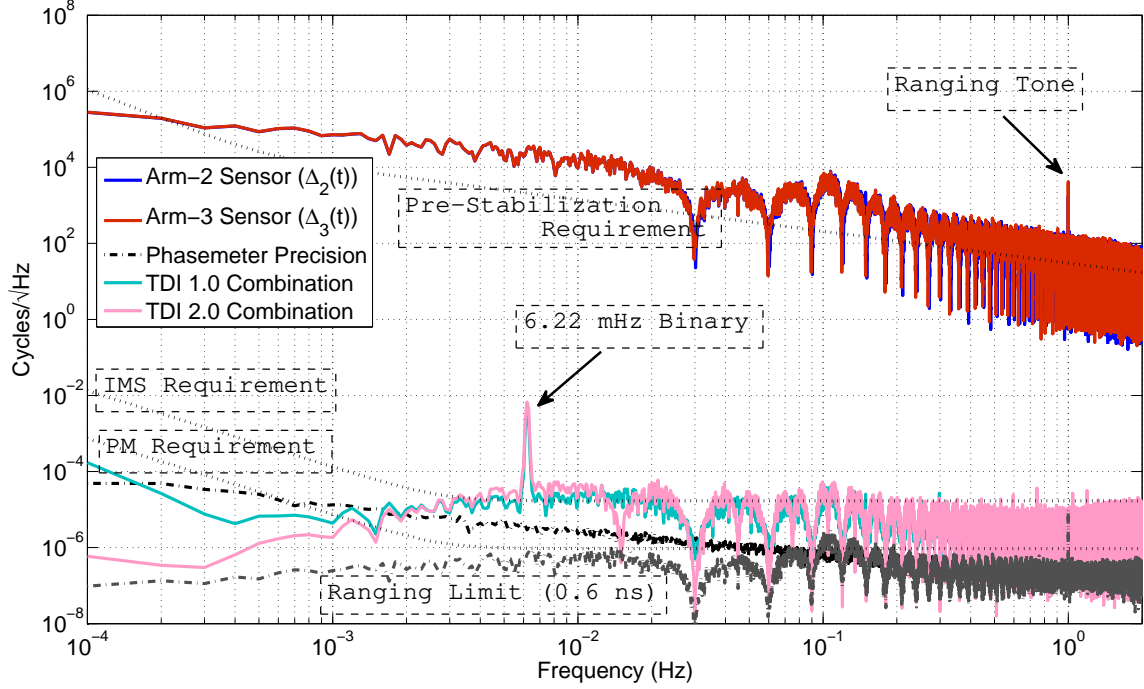


FIG. 5. Static Transponder (Baseline) Experimental Results: The sensor signals ($s_{21}(t) = \Delta_2(t)$, $s_{31}(t) = \Delta_3(t)$) are plotted along with the raw TDI- X_1 and TDI- X_2 results. The phasemeter measurement limitation and expected ranging limitations based on the calculated timing variance are also plotted.

reveal the phase-modulated GW binary at 6.22 mHz. The residual noise is dominated by phase noise added by the EPD units and, based on the timing-error, not by uncertainties in the ranging. The differences between the TDI- X_1 and TDI- X_2 combinations' spectral noise are caused by differences in their transfer functions with respect to the input laser phase noise. Fig.6 shows the spectra after the TDI combinations have been rescaled by their respective transfer function magnitude. Both agree well with each-other and demonstrate greater than 10 orders of magnitude laser frequency noise suppression below 1 mHz (Fig. 7).

Dynamic Arm Transponder (TDI 2.0 Verification)

In the next experiment, we incorporate time-dependent arm-lengths into the simulation with the β -values defined in Table II. Again, initially assuming $\beta = 0$, the 40000s measurements of the s_{21} and s_{31} signals are broken into 40, 1000s segments. These data segments

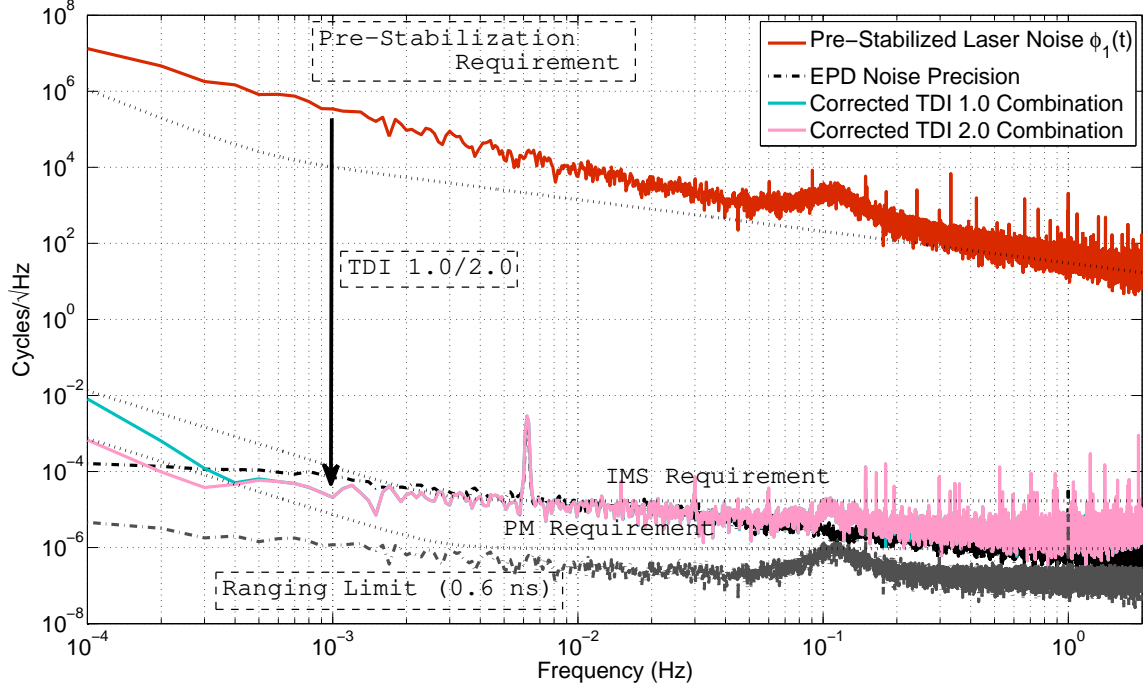


FIG. 6. Corrected Static Transponder (Baseline) Experimental Results: The input signal, $\phi_1(t)$, is plotted together with the TDI- X_1 and TDI- X_2 results, corrected by their respective transfer functions. Both TDI combinations are limited by the noise added by the EPD unit (dashed black curve).

are then used to minimize the ranging tone and calculate the round-trip time-delay for each segment as defined by Fig. 2. The linear regression of these time-delay offsets provides a first-order measure of the β to an accuracy of 100 ps/s as shown in Table III. The process also calculates a first order measure of the round-trip time delay with a ranging precision of $< 7.5 \mu\text{s}$ ($\sim 1.7 \text{ km}$) but, due to the incorrect $\beta = 0$ assumption, these values tend to equal the average delay for the data-segment. A second iteration improves the β accuracy to 80 fs/s and the ranging precision to $< 5.9 \text{ ns}$ ($\sim 1.8 \text{ m}$). The final iteration optimizes the β precision to 8.9 fs/s and the ranging precision to $< 0.65 \text{ ns}$ ($\sim 0.2 \text{ m}$). Producing comparable values to within the measurement error, additional iterations do little to improve the tone cancellation or ranging accuracy.

Applying the calculated round-trip functional values from the third iteration of the ranging procedure, we use the entire data-set to produce the TDI- X_1 and TDI- X_2 combinations (Fig. 8). The TDI- X_1 combination is limited, as theoretically anticipated, by Eq. 9 with

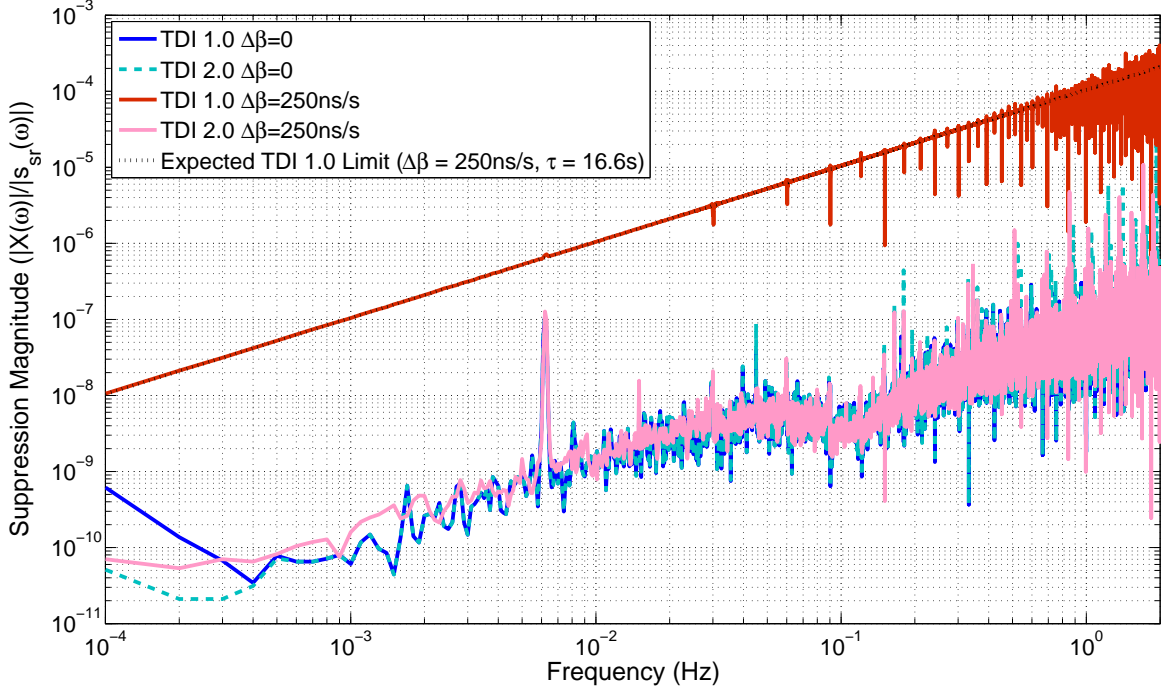


FIG. 7. Laser Noise Magnitude Suppression Function: The achieved transponder-measurement laser noise suppression magnitudes of the TDI- X_1 and TDI- X_2 combinations are plotted for both the static and dynamic experiments. The TDI- X_1 combination's noise suppression equals the theorized limit (Eq. 9).

$\tau \simeq 16.7$ s and $|\Delta\beta| = 250$ ns/s. The TDI- X_2 combination's correction terms account for this dynamic arm-length limitation and remove the velocity dependent laser phase noise resulting in a sensitivity equal to the experiment's baseline noise performance. This result meets the IMS requirement defined by the LISA mission concept design (Table I). The ranging precision, as plotted in Fig. 8, is not expected to be a limiting noise source which is verified with through the cross-correlation of the input noise with the TDI- X_2 combination as shown in Fig. 10.

Dynamic LISA-like (Phase-locked Laser, One-Way Ranging)

At this point, we include the phase-locking of the $L_{2/3}$ signals on the far spacecraft (Fig. 4) and the transmission of these phase signals back to the local-SC, thus generating and measuring all four s_{sr} beatnote observables. These signals are used in the same iterative

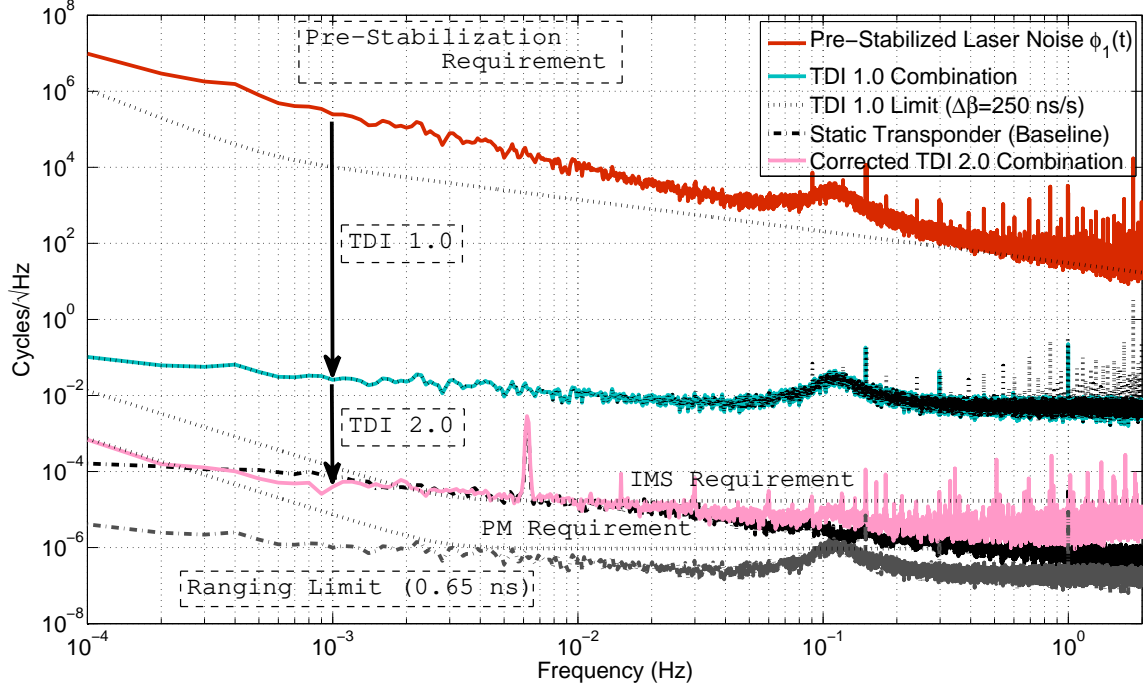


FIG. 8. Dynamic Transponder Experimental Results: The suppression of the TDI X_1 combination is limited by the arm-length time-dependence. The TDI X_2 combination removes the additional time-dependent-coupled laser noise and reveals the 6.22 mHz GW signal. As with the static case (Fig. 6), the EPD unit's phase transmission accuracy is the primary limiting noise source in the TDI combinations although, some sensitivity loss may occur due to a limited ranging capability around 100 mHz (Fig. 10).

process as previously described (Fig. 2, Table IV). The optimized time-delay functions from this process result in a measure of $|2\beta|$ to an accuracy better than ~ 70 fs/s and a round-trip ranging precision of ~ 5.0 ns (~ 1.5 m). The constraints on the one-way delay times through the residual PLL noise removal ($\sim 1/f$ mcycles/ $\sqrt{\text{Hz}}$) are not applicable until the precision of the round-trip delay times are accurate enough to remove enough of the input laser noise from the TDI combinations to reveal these residual PLL noises. Thus, it requires at least one iteration of the ranging process before one can constrain the one-way delay times. Applying a linear regression to the calculated one-way delay times we find a one-way ranging error of ~ 100 μs (~ 30 km). The outgoing and return delay times are unequal by $\sim 250 \pm 0.1$ ms, proving the ability to extract the individual one-way laser phase errors despite unequal delays along a single arm ($\tau_q(0) \neq \tau_{q'}(0)$).

TABLE IV. LISA-like Ranging Precision

TDI Experiment Name			
TDI-Ranging Constraint			
Iteration (TDI combination)	β	$\tau_{22'}(0), \tau_{33'}(0)$	$\delta\tau_{22'}, \delta\tau_{33'}$
Dynamic LISA-like			
Round-trip Ranging			
1 (TDI 2.0)	$2\beta_2 = -199.984 \text{ ns/s} \pm 12 \text{ ps/s}$	$\tau_{22'}(0) = 33.59821021 \text{ s} \pm 0.28 \mu\text{s}$	$\delta\tau_{22'} = 0.895 \mu\text{s}$
	$2\beta_3 = +300.052 \text{ ns/s} \pm 7.8 \text{ ps/s}$	$\tau_{33'}(0) = 33.21476669 \text{ s} \pm 0.18 \mu\text{s}$	$\delta\tau_{33'} = 0.568 \mu\text{s}$
2 (TDI 2.0)	$2\beta_2 = -200.000015 \text{ ns/s} \pm 71 \text{ fs/s}$	$\tau_{22'}(0) = 33.5982645303 \text{ s} \pm 1.6 \text{ ns}$	$\delta\tau_{22'} = 5.2 \text{ ns}$
	$2\beta_3 = +300.000013 \text{ ns/s} \pm 26 \text{ fs/s}$	$\tau_{33'}(0) = 33.2146434958 \text{ s} \pm 0.58 \text{ ns}$	$\delta\tau_{33'} = 1.9 \text{ ns}$
3 (TDI 2.0)	$2\beta_2 = -200.000028 \text{ ns/s} \pm 68 \text{ fs/s}$	$\tau_{22'}(0) = 33.5982645401 \text{ s} \pm 1.5 \text{ ns}$	$\delta\tau_{22'} = 5.0 \text{ ns}$
	$2\beta_3 = +300.000020 \text{ ns/s} \pm 25 \text{ fs/s}$	$\tau_{33'}(0) = 33.2146435166 \text{ s} \pm 0.58 \text{ ns}$	$\delta\tau_{33'} = 1.9 \text{ ns}$
One-Way Ranging			
3 (TDI 2.0)	$\beta_2 = -103.3 \text{ ns/s} \pm 1.4 \text{ ns/s}$	$\tau_2(0) = 16.68021 \text{ s} \pm 32 \mu\text{s}$	$\delta\tau_2 = 105 \mu\text{s}$
		$\tau_{2'}^*(0) = 16.91805 \text{ s} \pm 32 \mu\text{s}$	$\delta\tau_{2'} = 105 \mu\text{s}$
	$\beta_3 = +152.24 \text{ ns/s} \pm 1.4 \text{ ns/s}$	$\tau_3(0) = 16.48824 \text{ s} \pm 31 \mu\text{s}$	$\delta\tau_3 = 99 \mu\text{s}$
		$\tau_{3'}^*(0) = 16.72640 \text{ s} \pm 31 \mu\text{s}$	$\delta\tau_{3'} = 99 \mu\text{s}$
Dynamic LISA-like			
with Confusion Noise			
Round-trip Ranging			
3 (TDI 2.0)	$2\beta_2 = -199.999991 \text{ ns/s} \pm 50 \text{ fs/s}$	$\tau_{22'}(0) = 33.6012734891 \text{ s} \pm 1.1 \text{ ns}$	$\delta\tau_{22'} = 3.7 \text{ ns}$
	$2\beta_3 = +300.000137 \text{ ns/s} \pm 22 \text{ fs/s}$	$\tau_{33'}(0) = 33.2100302983 \text{ s} \pm 0.49 \text{ ns}$	$\delta\tau_{33'} = 1.6 \text{ ns}$
One-Way Ranging			
3 (TDI 2.0) ‡	$\beta_2 = -96.81 \text{ ns/s} \pm 2.3 \text{ ns/s}$	$\tau_2(0) = 16.73546 \text{ s} \pm 53 \mu\text{s}$	$\delta\tau_2 = 169 \mu\text{s}$
		$\tau_{2'}^*(0) = 16.86582 \text{ s} \pm 53 \mu\text{s}$	$\delta\tau_{2'} = 169 \mu\text{s}$
	$\beta_3 = +149.439 \text{ ns/s} \pm 1.4 \text{ ns/s}$	$\tau_3(0) = 16.53994 \text{ s} \pm 32 \mu\text{s}$	$\delta\tau_3 = 102 \mu\text{s}$
		$\tau_{3'}^*(0) = 16.67009 \text{ s} \pm 32 \mu\text{s}$	$\delta\tau_{3'} = 102 \mu\text{s}$

‡ The additional error in the one-way confusion noise measurement as compared to the phase-locked measurement is expected to be due to the coupling of low-frequency noise using the minimized-RMS ranging method [15].

* The returning delay times tend to be longer than the outgoing delay times by 100-300 ms as a result of internal delays within the DSP system's EPD units.

Applying these optimized one-way functional values from the ranging procedure, we produce the TDI- X_1 and TDI- X_2 combinations (Fig. 9). Again, the TDI- X_1 combination equals the expected limitation (Eq. 9). The TDI- X_2 combination meets the LISA IMS requirement to within a factor of 4. Based on the variance of the fitted delay times, the ranging preci-

sions are not a limiting noise source as plotted in Fig. 9. The cross-correlation of the TDI- X_2 combination with the laser and PLL noise sources (Fig. 10) indicates that all the known and accounted-for noise sources have been sufficiently removed from the interferometer’s output. Thus, the TDI noise cancellation limitation likely results from the combination of multiple PM and EPD clock-noise sources in these LISA-like measurements resulting in a sensitivity greater than the simulator’s baseline performance.

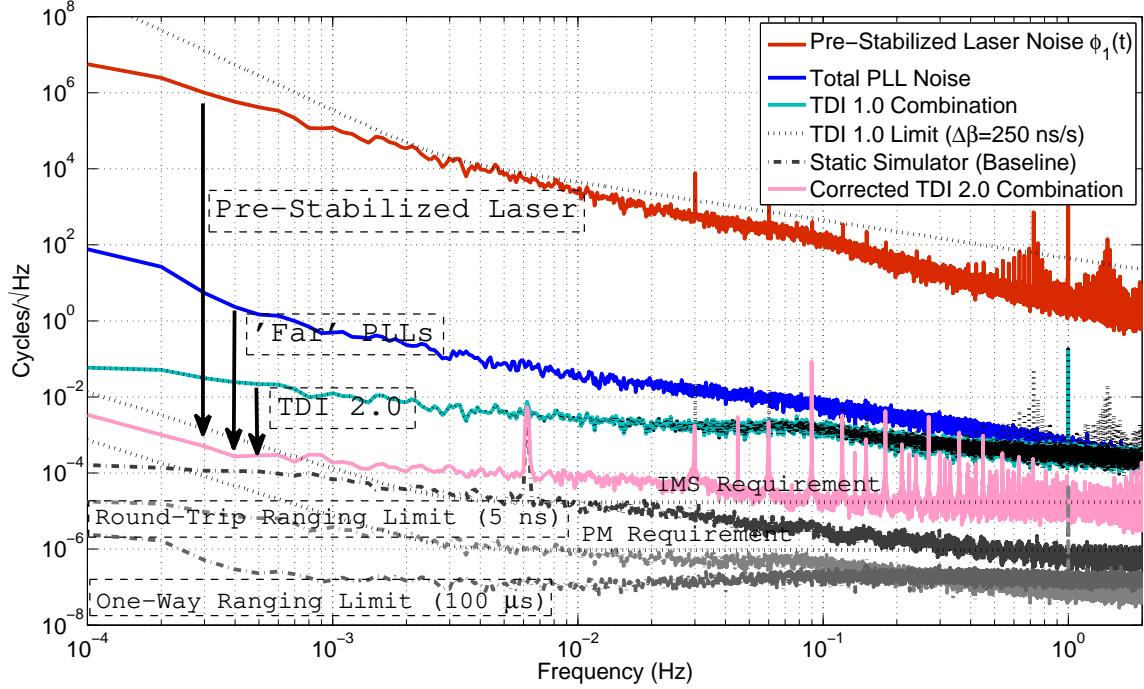


FIG. 9. Dynamic LISA-like (Phase-locked) Experimental Results: The suppression of the TDI X_1 combination is limited by the expected arm-length time-dependence. The TDI X_2 combination removes the input laser noise, the far-SC PLL residual phase noise, and the time-dependent coupled laser noise to reveal the 6.22 mHz GW signal. The sensitivity limitation comes, most likely, as a result of multiple uncorrelated PM and EPD clock noise sources.

Dynamic LISA-like (with Confusion Noise Background)

Lastly, we include a low frequency simulated ‘confusion noise’ into the measurement to ensure that these low-frequency terms do not limit the ranging precision. The confusion noise background, $\simeq 6.4/(f\sqrt{1+(f/f_R)^2}) \mu\text{cycles}/\sqrt{\text{Hz}}$ where $f_R = 1 \text{ mHz}$, and the 6.22 mHz

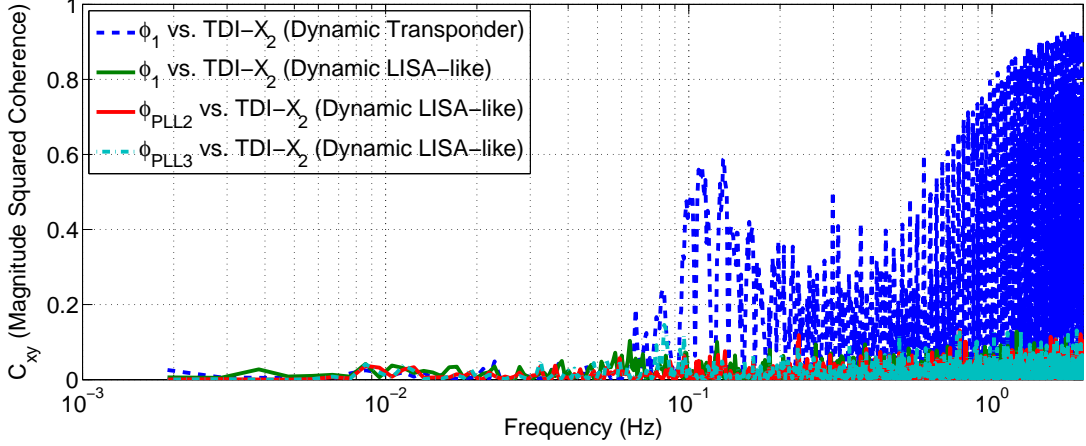


FIG. 10. TDI vs. Input Cross Correlation: The magnitude squared cross-correlation of the LISA-like TDI measurements show no correlation with the input noise or either PLL noise source, verifying that all the laser noise sources have been sufficiently removed. The cross-correlation of the dynamic transponder TDI measurement shows some input phase correlated noise cancellation limitation for frequencies above 100 mHz.

mono-chromatic binary are simultaneously injected. The optimized ranging result places bounds on the $|2\beta|$ accuracy better than ~ 50 fs/s and produces a round-trip ranging precision of ~ 3.7 ns (~ 1.1 m). Thus, this confusion noise result achieves a ranging precision on the same order as the simulator's phase-locked performance, indicating that low-frequency noise has little to no effect on the ranging tone cancellation or the measured arm-lengths.

The time-series of the extracted monochromatic GW binary signal using the TDI- X_2 combination is plotted in Fig. 12 with and without the confusion noise background. Given the injected $51.2 \mu\text{cycle}$ EPD GW-signal and comparing the measured amplitude with the expected GW amplitude we find the TDI- X_2 extracted signal matches the expected amplitude of $2 \times 2.33 \times 51.2 \mu\text{cycles} = 238 \mu\text{cycles}$. The factor of 2 accounts for the two interferometer arms while the factor of 2.33 accounts for the TDI transfer function's signal gain at $f = 6.22$ mHz ($|\tilde{X}_2(6.22 \text{ mHz})| = 2.33$).

The noise spectrum comparisons between the TDI- X_2 outputs of the dynamic LISA-like experiments, with and without the confusion noise background, are plotted in Fig. 11 to show the additional low-frequency noise. These spectra are a factor of 5 larger than the simulator's baseline performance. Again, this likely results from the extra uncorrelated phasemeter and EPD clock noise terms in addition to double the number of s_{sr} observable terms used to

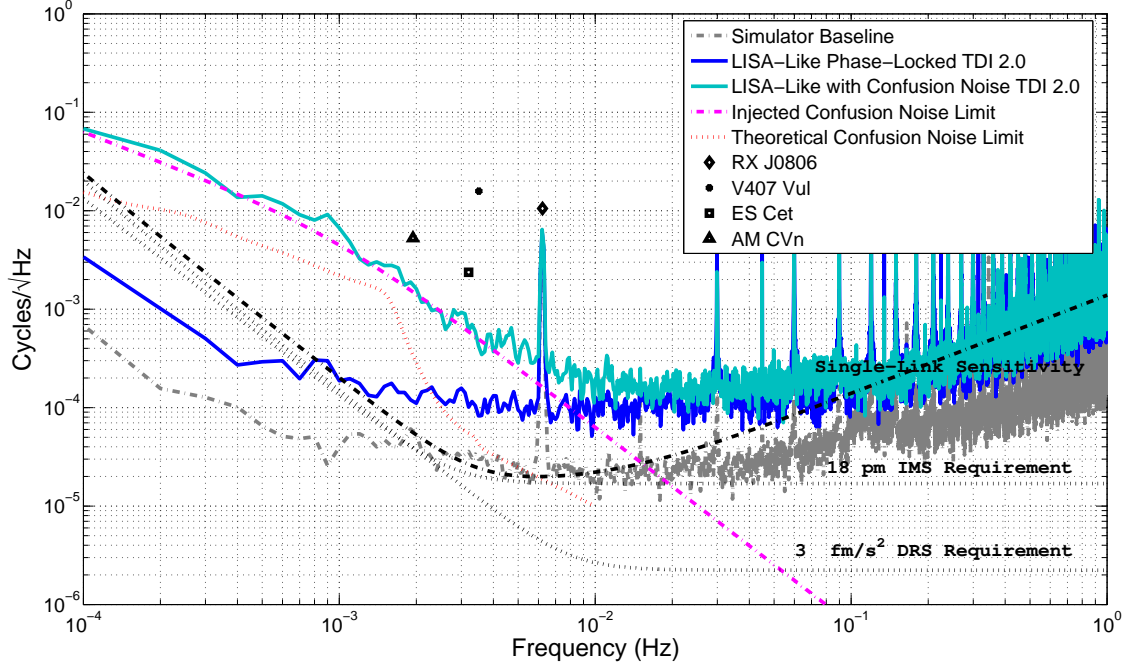


FIG. 11. Compiled Results, Comparison with TDI for LISA: In this figure we have compiled the results of the TDI simulations and attempt to make a direct comparison with the expected LISA strain sensitivity. The DRS and IMS requirement are root-square summed and scaled by the high-frequency LISA GW-sensitivity loss function to produce the effective single-link LISA sensitivity. The baseline spectral noise of the UFLIS simulator (grey-blue) from the TDI-Transponder measurements is plotted. The velocity corrected TDI- $X_{2.0}$ spectrum of the dynamic arm TDI simulation with (cyan) and without (blue) the injected binary confusion noise (dotted-magenta) are also plotted. For a direct comparison to the IMS sensitivity requirement, these three TDI measurements are scaled to account for the high-frequency GW-sensitivity loss expected in LISA. An estimate of the confusion noise limit is shown (dotted-red) along with the four brightest verification binaries rescaled from a 1-year averaged strain sensitivity to noise spectra in $\text{cycles}/\sqrt{\text{Hz}}$. The strain magnitude of the 1 year averaged RX-J0806 binary and the 10000 s EPD injected GW have amplitudes such that they result in similar LSD amplitudes in this figure.

form the TDI combinations in these LISA-like experiments. All three measured spectra in Fig. 11 have been scaled by the high-frequency sensitivity loss ‘roll-up’ of the LISA-detector

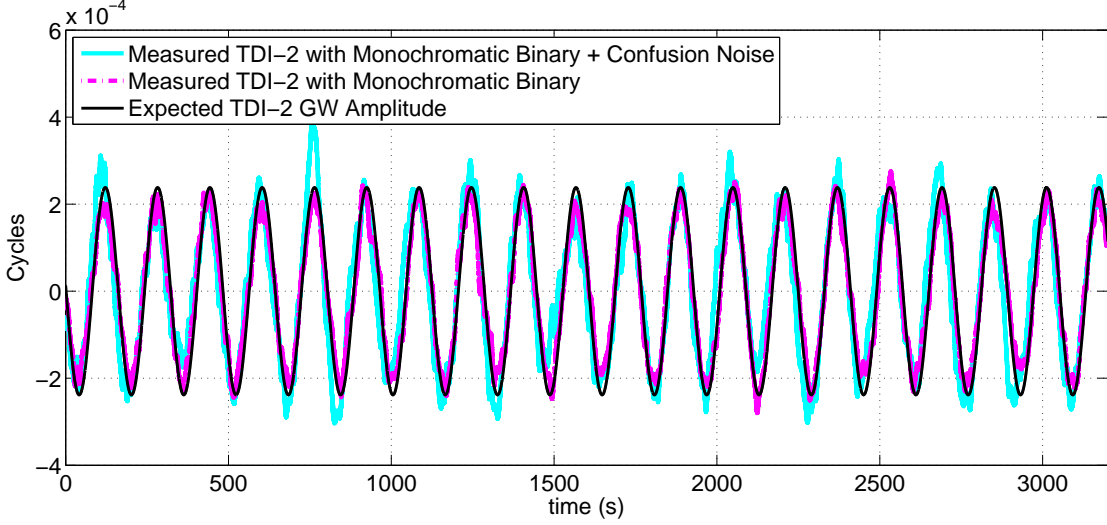


FIG. 12. TDI- X_2 Time-Series: The TDI- X_2 extracted signals match the expected GW amplitude given the $51.2 \mu\text{cycle}$ GW EPD injection amplitude after scaling by the magnitude of the TDI- X_2 combination's transfer function evaluated at $f = 6.22 \text{ mHz}$, $|\tilde{X}_2(6.22 \text{ mHz})| = 2.33$.

for GW-frequencies $f > 12 \text{ mHz}$, given by:

$$T(f) = \sqrt{1 + \left(\frac{f}{12 \text{ mHz}}\right)^2},$$

in order to obtain a direct comparison with the single-link sensitivity. The injected confusion noise background is plotted and matches the spectrum of measured confusion noise. A theoretical confusion-noise background [28] and the expected 1-year strain amplitude of the four strongest LISA verification binaries [27] are marked for additional reference.

CONCLUSION

Following the initial interferometry tests of a static LISA model [14], we expanded UFLIS and added time varying signal travel times, Doppler shifts, and gravitational wave signals to our electronic phase delay units. This enables tests of the LISA interferometry in a realistic, dynamic model. Our experimental results show that than 10 orders of magnitude of laser frequency noise can be canceled using appropriately time-shifted data streams in the TDI- X_2 data combination. We also developed and demonstrated a simple but powerful ranging method to measure the signal travel times between the spacecraft.

We verified that the ability to reduce laser frequency noise using a TDI- X_1 data combination is indeed limited by the relative velocities between the spacecraft. Furthermore, we demonstrated the removal of the residual phase lock loop noise added at the far spacecraft and, in this configuration, showed that the requirements on one-way ranging are relaxed by several orders of magnitude compared to the requirements on round trip ranging.

In the process, we developed and tested data analysis tools which take the raw phasemeter data streams, extracts the light-travel time functions, and generates the TDI- X_2 data sets. We also added a confusion noise GW-background to our interferometry emulator and verified that this background noise does not interfere with our ranging capabilities.

Future experiments should include real, LISA-like GW signals using data-sets generated with LISA-tools like Synthetic LISA [9]. Simulations with three independently stabilized lasers might also be valuable towards verifying the constraints on the one-way ranging capabilities.

%

* smitryk@phys.ufl.edu.

- [1] O. Jennrich *et al.*, *NGO assessment study report (Yellow Book): ESA/SRE(2011)19*, Tech. Rep. (2012) <http://sci.esa.int/science-e/www/object/index.cfm?fobjectid=49839#>
- [2] “Concepts for the nasa gravitational-wave mission,” (Sept 2011), nSPIRES-NASA Request for Information: NNH11ZDA019L
- [3] K. Danzmann, T. Prince, *et al.*, *LISA Science Requirements Document, v3.0*, Tech. Rep. (2005) http://list.caltech.edu/lib/exe/fetch.php?media=documents:requirements:srd_v3_0_sb.pdf
- [4] P. Bender, K. Danzmann, *et al.*, *LISA: Pre-Phase A Report*, Tech. Rep. (1998) <http://list.caltech.edu/lib/exe/fetch.php?media=documents:early:prephasea.pdf>
- [5] K. Danzmann, T. Prince, *et al.*, *LISA assessment study report (Yellow Book)*, Tech. Rep. (2011) <http://sci.esa.int/science-e/www/object/index.cfm?fobjectid=48364#>
- [6] *Laser Interferometer Space Antenna (LISA) Mission Concept*, Tech. Rep. LISA-PRJ-RP-0001 (NASA, ESA, 2009) <http://lisa.gsfc.nasa.gov/Documentation/LISA-PRJ-RP-0001.pdf>
- [7] J. W. Armstrong, F. B. Estabrook, and M. Tinto, *Astrophys. J.* **527**, 814 (Dec. 1999)
- [8] L. J. Rubbo, N. J. Cornish, and O. Poujade, *Phys. Rev. D* **69**, 082003 (Apr. 2004),

- [9] M. Vallisneri, Phys. Rev. D **71**, 022001 (Jan. 2005), arXiv:gr-qc/0407102
- [10] K. A. Arnaud, G. Auger, S. Babak, J. G. Baker, M. J. Benacquista, E. Bloomer, D. A. Brown, J. B. Camp, J. K. Cannizzo, N. Christensen, J. Clark, N. J. Cornish, J. Crowder, C. Cutler, L. S. Finn, H. Halloin, K. Hayama, M. Hendry, O. Jeannin, A. Królak, S. L. Larson, I. Mandel, C. Messenger, R. Meyer, S. Mohanty, R. Nayak, K. Numata, A. Petiteau, M. Pitkin, E. Plagnol, E. K. Porter, R. Prix, C. Roever, A. Stroeer, R. Thirumalainambi, D. E. Thompson, J. Toher, R. Umstaetter, M. Vallisneri, A. Vecchio, J. Veitch, J.-Y. Vinet, J. T. Whelan, and G. Woan, Classical and Quantum Gravity **24**, 529 (Oct. 2007), arXiv:gr-qc/0701139
- [11] S. Babak, J. G. Baker, M. J. Benacquista, N. J. Cornish, J. Crowder, C. Cutler, S. L. Larson, T. B. Littenberg, E. K. Porter, M. Vallisneri, A. Vecchio, t. M. L. data challenge task force, G. Auger, L. Barack, A. Blaut, E. Bloomer, D. A. Brown, N. Christensen, J. Clark, S. Fairhurst, J. R. Gair, H. Halloin, M. Hendry, A. Jimenez, A. Królak, I. Mandel, C. Messenger, R. Meyer, S. Mohanty, R. Nayak, A. Petiteau, M. Pitkin, E. Plagnol, R. Prix, E. L. Robinson, C. Roever, P. Savov, A. Stroeer, J. Toher, J. Veitch, J. Vinet, L. Wen, J. T. Whelan, G. Woan, and t. Challenge-2 participants, Classical and Quantum Gravity **25**, 114037 (Jun. 2008), arXiv:0711.2667 [gr-qc]
- [12] G. de Vine, B. Ware, K. McKenzie, R. E. Spero, W. M. Klipstein, and D. A. Shaddock, Physical Review Letters **104**, 211103 (May 2010), arXiv:1005.2176 [astro-ph.IM]
- [13] R. J. Cruz, J. I. Thorpe, A. Preston, R. Delgadillo, M. Hartman, S. Mitryk, A. Worley, G. Boothe, S. R. Guntaka, S. Klimenko, D. B. Tanner, and G. Mueller, Classical and Quantum Gravity **23**, 751 (Oct. 2006)
- [14] S. J. Mitryk, V. Wand, and G. Mueller, Classical and Quantum Gravity **27**, 084012 (Apr. 2010)
- [15] M. Tinto, M. Vallisneri, and J. W. Armstrong, Phys. Rev. D **71**, 041101 (Feb. 2005), arXiv:gr-qc/0410122
- [16] M. Armano, M. Benedetti, J. Bogenstahl, D. Bortoluzzi, P. Bosetti, N. Brandt, A. Cavalleri, G. Ciani, I. Cristofolini, A. M. Cruise, K. Danzmann, I. Diepholz, G. Dixon, R. Dolesi, J. Fauste, L. Ferraioli, D. Fertin, W. Fichter, M. Freschi, A. García, C. García, A. Grynagier, F. Guzmán, E. Fitzsimons, G. Heinzl, M. Hewitson, D. Hollington, J. Hough, M. Hueller, D. Hoyland, O. Jennrich, B. Johlander, C. Killow, A. Lobo, D. Mance, I. Mateos, P. W.

- McNamara, A. Monsky, D. Nicolini, D. Nicolodi, M. Nofrarias, M. Perreux-Lloyd, E. Plagnol, G. D. Racca, J. Ramos-Castro, D. Robertson, J. Sanjuan, M. O. Schulte, D. N. A. Shaul, M. Smit, L. Stagnaro, F. Steier, T. J. Sumner, N. Tateo, D. Tombolato, G. Vischer, S. Vitale, G. Wanner, H. Ward, S. Waschke, V. Wand, P. Wass, W. J. Weber, T. Ziegler, and P. Zweifel, *Classical and Quantum Gravity* **26**, 094001 (May 2009)
- [17] R. Fleddermann, F. Steier, M. Tröbs, J. Bogenstahl, C. Killow, G. Heinzel, and K. Danzmann, *Journal of Physics Conference Series* **154**, 012022 (Mar. 2009)
- [18] D. A. Shaddock, M. Tinto, F. B. Estabrook, and J. W. Armstrong, *Phys. Rev. D* **68**, 061303 (Sep. 2003), [arXiv:gr-qc/0307080](#)
- [19] D. A. Shaddock, *Classical and Quantum Gravity* **25**, 114012 (Jun. 2008)
- [20] N. J. Cornish and R. W. Hellings, *Classical and Quantum Gravity* **20**, 4851 (Nov. 2003), [arXiv:gr-qc/0306096](#)
- [21] J. José Esteban, I. Bykov, A. Francisco García Marín, G. Heinzel, and K. Danzmann, *Journal of Physics Conference Series* **154**, 012025 (Mar. 2009)
- [22] M. Tinto, D. A. Shaddock, J. Sylvestre, and J. W. Armstrong, *Phys. Rev. D* **67**, 122003 (Jun. 2003), [arXiv:gr-qc/0303013](#)
- [23] D. A. Shaddock, B. Ware, R. E. Spero, and M. Vallisneri, *Phys. Rev. D* **70**, 081101 (Oct. 2004), [arXiv:gr-qc/0406106](#)
- [24] R. W. P. Drever, J. L. Hall, F. V. Kowalski, J. Hough, G. M. Ford, A. J. Munley, and H. Ward, *Applied Physics B: Lasers and Optics* **31**, 97 (Jun. 1983)
- [25] S. Mitryk, *Laser Noise Mitigation Through Time Delay Interferometry for space-based Gravitational Wave Interferometers Using the UF Laser Interferometry Simulator*, Ph.D. thesis, University of Florida (2012)
- [26] S. Barke, M. Tröbs, B. Sheard, G. Heinzel, and K. Danzmann, *Applied Physics B: Lasers and Optics* **98**, 33 (Jan. 2010)
- [27] A. Stroeer and A. Vecchio, *Classical and Quantum Gravity* **23**, 809 (Oct. 2006), [arXiv:astro-ph/0605227](#)
- [28] P. L. Bender and D. Hils, *Classical and Quantum Gravity* **14**, 1439 (Jun. 1997)